Journal for ImmunoTherapy of Cancer

Preclinical development of novel PD-L1 tracers and first-in-human study of [^{68}Ga]Ga-NOTA-RW102 in patients with lung cancers

You Zhang,[1] Min Cao,[2] Yanfei Wu,[3] Sara Malih,[4,5] Dong Xu,[6] Erpeng Yang,[1] Muhsin H Younis,[4] Wilson Lin,[4] Haitao Zhao ,[1] Cheng Wang,[1] Qiufang Liu,[7] Jonathan W Engle,[4] Mohammad J Rasaee,[5] Yihui Guan,[3] Gang Huang,[1] Jianjun Liu,[1] Weibo Cai,[4] Fang Xie,[3] Weijun Wei [1]

To cite: Zhang Y, Cao M, Wu Y, *et al*. Preclinical development of novel PD-L1 tracers and first-in-human study of [^{68}Ga]Ga-NOTA-RW102 in patients with lung cancers. *Journal for ImmunoTherapy of Cancer* 2024;**12**:e008794. doi:10.1136/jitc-2024-008794

► Additional supplemental material is published online only. To view, please visit the journal online (https://doi.org/10.1136/jitc-2024-008794).

YZ, MC and YW contributed equally.

Accepted 20 March 2024

For numbered affiliations see end of article.

Correspondence to
Professor Weijun Wei; wwei@shsmu.edu.cn

Fang Xie; fangxie@fudan.edu.cn

Professor Jianjun Liu; nuclearj@163.com

Dr Weibo Cai; wcai@uwhealth.org

ABSTRACT

Background The programmed cell death protein-1 (PD-1)/programmed death receptor ligand 1 (PD-L1) axis critically facilitates cancer cells' immune evasion. Antibody therapeutics targeting the PD-1/PD-L1 axis have shown remarkable efficacy in various tumors. Immuno-positron emission tomography (ImmunoPET) imaging of PD-L1 expression may help reshape solid tumors' immunotherapy landscape.

Methods By immunizing an alpaca with recombinant human PD-L1, three clones of the variable domain of the heavy chain of heavy-chain only antibody (VHH) were screened, and RW102 with high binding affinity was selected for further studies. ABDRW102, a VHH derivative, was further engineered by fusing RW102 with the albumin binder ABD035. Based on the two targeting vectors, four PD-L1-specific tracers ([^{68}Ga]Ga-NOTA-RW102, [^{68}Ga]Ga-NOTA-ABDRW102, [^{64}Cu]Cu-NOTA-ABDRW102, and [^{89}Zr]Zr-DFO-ABDRW102) with different circulation times were developed. The diagnostic efficacies were thoroughly evaluated in preclinical solid tumor models, followed by a first-in-human translational investigation of [^{68}Ga]Ga-NOTA-RW102 in patients with non-small cell lung cancer (NSCLC).

Results While RW102 has a high binding affinity to PD-L1 with an excellent K_D value of 15.29 pM, ABDRW102 simultaneously binds to human PD-L1 and human serum albumin with an excellent K_D value of 3.71 pM and 3.38 pM, respectively. Radiotracers derived from RW102 and ABDRW102 have different *in vivo* circulation times. In preclinical studies, [^{68}Ga]Ga-NOTA-RW102 immunoPET imaging allowed same-day annotation of differential PD-L1 expression with specificity, while [^{64}Cu]Cu-NOTA-ABDRW102 and [^{89}Zr]Zr-DFO-ABDRW102 enabled longitudinal visualization of PD-L1. More importantly, a pilot clinical trial shows the safety and diagnostic value of [^{68}Ga]Ga-NOTA-RW102 immunoPET imaging in patients with NSCLCs and its potential to predict immune-related adverse effects following PD-L1-targeted immunotherapies.

Conclusions We developed and validated a series of PD-L1-targeted tracers. Initial preclinical and clinical evidence indicates that immunoPET imaging with [^{68}Ga]Ga-NOTA-RW102 holds promise in visualizing differential PD-L1 expression, selecting patients for PD-L1-targeted immunotherapies, and monitoring immune-related adverse effects in patients receiving PD-L1-targeted treatments.

Trial registration number NCT06165874.

WHAT IS ALREADY KNOWN ON THIS TOPIC

⇒ Programmed death receptor ligand 1 (PD-L1)-targeted antibody therapeutics are effective for some tumors, but patient response varies. Molecular imaging of PD-L1 expression can aid in patient selection and response prediction.

WHAT THIS STUDY ADDS

⇒ This study introduces four VHH-derived immuno-positron emission tomography (immunoPET) imaging tracers with varying circulation times. Clinical translation of [^{68}Ga]Ga-NOTA-RW102 demonstrates its ability to visualize differential PD-L1 expression and its potential to predict immune-related adverse events.

HOW THIS STUDY MIGHT AFFECT RESEARCH, PRACTICE OR POLICY

⇒ [^{68}Ga]Ga-NOTA-RW102 immunoPET imaging may improve the clinical use of PD-L1-targeted therapeutics by patient selection, treatment response and adverse events monitoring.

BACKGROUND

Immunotherapies, including immune checkpoint inhibitors, cancer vaccines, and cell therapies, continuously shape the landscape of cancer therapies. Programmed death receptor ligand 1 (PD-L1) is an immune checkpoint that interacts with the receptor programmed death 1 (PD-1) on T cells, inhibiting T-cell activation and suppressing antitumor immunity. Immune checkpoint blockade with antibodies targeting the PD-1/PD-L1 axis has prolonged survival in

patients with cancer. With the availability of these treatment options, clinicians are faced with challenges in non-invasive PD-L1 assessment, precise patient selection, and timely response assessment after administering antibody therapeutics.

With the increasingly approved therapeutic antibodies and commercial supply of long-lived radionuclides such as zirconium-89 (^{89}Zr) and copper-64 (^{64}Cu), immuno-positron emission tomography (immunoPET) imaging with radiolabeled monoclonal antibodies (mAbs) and antibody fragments has fulfilled some of the tasks by visualizing target expression.[1] ImmunoPET imaging with mAb-based tracers offers several advantages, such as safety profiles, easy access, availability in large amounts, and robust labeling protocols. However, their slow clearance, less optimal tumor-to-background ratio, poor penetration in the tumor interstitium, long imaging period lasting over a week, and noticeable radiation dose to patients are practical considerations that hinder their routine clinical use. In this setting, immunoPET imaging with radiolabeled single-domain antibodies has rapidly evolved.[2–4] The variable domain of the heavy chain of heavy-chain only antibody (VHH or NANOBODY) is the smallest antibody fragment with a molecular size of ~15 kDa. It is highly stable and has a high affinity, which makes it efficient in extravasation. It is a valuable tool in antibody research and developing same-day immunoPET imaging tracers due to its versatile engineering potentials. For instance, two HER2-specific nanobody tracers have been translated for clinical use.[5 6]

Up to now, mAbs and nanobodies have been radiolabeled for non-invasive imaging of PD-L1 expression. ^{89}Zr-atezolizumab was tested in 22 patients with either bladder cancer, triple-negative breast cancer, or non-small cell lung cancer (NSCLC) before atezolizumab therapy. Despite the high but variable uptake of ^{89}Zr-atezolizumab in tumors, PD-L1 status revealed by ^{89}Zr-atezolizumab, but not by immunohistochemistry (IHC) or RNA-sequencing-based approaches, correlated with clinical responses of atezolizumab treatment,[7] possibly due to inherent artifacts of IHC such as tissue sampling errors and inequivalent interpretation of the staining results.[8] Xing *et al* developed the nanobody-derived PD-L1-targeting ^{99m}Tc-NM-01. They reported the physiological uptake of the tracer in the liver, spleen, and, to a lesser extent, in the bone marrow and lungs. The translational study showed intratumoral and intertumoral heterogeneity of PD-L1 expression and a good correlation between the SPECT signal and IHC staining results.[9] While ^{99m}Tc-labeled tracers have good availabilities, the low spatial resolution and lack of quantitation with SPECT are practical challenges in precisely quantifying PD-L1. To this end, ^{68}Ga-labeled nanobody tracers targeting PD-L1 have been developed.[10–12] Envafolimab (KN035) is a nanobody derivative specially engineered for treating late-stage solid tumors. This drug has a molecular weight of 79.6 kDa and is approved for treating late-stage biliary tract carcinoma and soft tissue sarcoma in the USA, as well as late-stage solid tumors in China. Li *et al* developed ^{89}Zr-Df-KN035 and reported the diagnostic efficacy in glioma xenografts and the circulation profiles in non-human primates.[13] An original research was recently published reporting the imaging safety and biodistribution profiles of ^{89}Zr-Df-KN035 in patients with PD-L1-positive solid tumors (NCT04977128).[14] However, the use of both ^{89}Zr-atezolizumab and ^{89}Zr-Df-KN035 in routine clinical practice is inconvenient, and same-day molecular imaging remains the mainstay of clinical practice.

Apart from selecting patients and monitoring the dynamics of PD-L1 in the course of immunotherapies, how to non-invasively detect immune-related side effects is another clinical challenge. Currently, limited evidence supports PD-L1-targeted imaging in visualizing immune-related side effects.[15–17] In this study, our primary objective is to develop novel nanobody-derived tracers that have high affinity and can annotate PD-L1 with varying pharmacokinetics. We also aim to identify a promising tracer for clinical use, explore its potential to visualize PD-L1 expression and monitor immune-related adverse events (irAEs) following PD-L1-targeted treatments.

METHODS

Production and purification of RW102 and ABDRW102

A healthy alpaca was immunized with 2 mg of recombinant human PD-L1 protein (Cat: 10084-H08H; Sino Biological) mixed with an equal volume of Freund's complete adjuvant six times. Meanwhile, the extracellular domain of human PD-L1 fused to Fc (1 mg mixed with Freund's complete adjuvant) was used to immunize Xinjiang Bactrian camel three to seven times. Phage display technology was used to obtain the positive clones, followed by next-generation sequencing of the selected clones. RW101, RW102, and RW103 sequences were cloned into pET-30a(+) and expressed in BL21(DE3) competent cells. The N-terminal tag (HHHHHH) was inserted into the nanobody sequence for purification. ABDRW102 was further developed by fusing RW102 with the albumin binder (ABD035) derived from the Streptococcal protein G with a flexible $(G_4S)_3$ linker and expressed in CHO cells as we previously reported.[18] The purity of the proteins was examined by sodium dodecyl sulfate-polyacrylamide gel electrophoresis (SDS-PAGE).

Surface plasmon response

The affinity of RW102, RW103, and ABDRW102 binding to human PD-L1 protein (PD1-H5229, ACROBiosystems) was tested by surface plasmon resonance (SPR). All measurements were performed on a Biacore T200 device (GE HealthCare) at 25°C with HEPES-buffered saline (0.01 M HEPES pH 7.4, 0.15 M NaCl, three mM ethylenediaminetetraacetic acid, 0.005% Tween 20) as the running buffer. Briefly, different dilutions of samples to be tested were run at 50 µL/min on a CM5 sensor chip with a high density of human PD-L1 protein, and specific binding signals (response units) were recorded. Samples

were allowed to bind with the target protein for 300 s, and dissociation was monitored for 180 s. The equilibrium dissociation constant K_D was calculated by fitting the obtained sensor grams to theoretical curves using Biacore Evaluation software. Also, the binding affinity of NOTA-RW102, NOTA-ABDRW102, and DFO-ABDRW102 to human PD-L1 protein, the binding affinity of ABDRW102 to human serum albumin (HSA) and murine serum albumin (MSA), the binding affinity of RW102 and NOTA-RW102 to murine PD-L1 (PD1-M5220, ACROBiosystems) were determined similarly.

Cell lines and animal models

By immunohistochemical screening of multiple tumor tissues for PD-L1 expression, four tumor cell lines and a clear cell renal cell carcinoma PDX model (No. 62 PDX) were selected for the imaging experiments. The colon cancer cell line RKO was chosen for [^{68}Ga]Ga-NOTA-RW102, [^{68}Ga]Ga-NOTA-ABDRW102, and [^{64}Cu]Cu-NOTA-ABDRW102 imaging. The PD-L1-overexpression metastatic hepatocellular carcinoma cell line LM3-PD-L1 was selected for [^{68}Ga]Ga-NOTA-RW102 and [^{89}Zr]Zr-DFO-ABDRW102 imaging. The PD-L1-negative No. 62 PDX and T3-M4 pancreatic cancer cell line models were used for [^{68}Ga]Ga-NOTA-RW102 imaging. To further confirm the specificity of targeting, [^{68}Ga]Ga-NOTA-RW102 blocking studies were conducted using models established from A375-PD-L1, a melanoma cell line overexpressing PD-L1. The cell lines were purchased from the American Type Culture Collection (Manassas, Virginia, USA) and cultured in Dulbecco's modified Eagle's medium at 37°C with 5% CO_2. Also added to the media were 10% fetal bovine serum (GE HealthCare, Chicago, Illinois, USA) and 1% Pen-Strep (Invitrogen).

Female BALB/c nude mice (4–5 weeks of age) were purchased from Renji Hospital Experimental Animal Center (Shanghai, China). NCG mice (NOD-Prkdcem^{26Cd52}Il2rgem^{26Cd22}/Nju) were purchased from the National Model Animal Resource Information Platform (#T001475, Nanjing University, China) for establishing No. 62 PDX models. All animal experiments were performed following the guidelines of the Institutional Animal Care and Use Committee (#2023–442; Renji Hospital, School of Medicine, Shanghai Jiao Tong University). To establish subcutaneous tumor models, about 1–5×10^6 of RKO, LM3-PD-L1, A375-PD-L1 or T3-M4 tumor cells in 100 µL phosphate buffer saline were inoculated subcutaneously into the right front flanks of the mice, respectively. The animals were used for *in vivo* imaging studies when the tumor volume reached 200–300 mm^3 (2–3 weeks after inoculation).

Chelator conjugation, radiometal labeling, and quality control

For ^{68}Ga and ^{64}Cu labeling, RW102 and ABDRW102 were conjugated with the bifunctional chelator *p*-SCN-Bn-NOTA (B-605, Macrocyclics) with a molar ratio of 1:10. For ^{89}Zr-labeling, ABDRW102 was conjugated with the bifunctional chelator *p*-SCN-Bn-Deferoxamine (B-705, Macrocyclics) similarly. ^{89}Zr was produced freshly at Renji Hospital, while ^{64}Cu was produced at the University of Wisconsin–Madison, as previously reported.[19] For ^{68}Ga-labeling, 370–555 MBq of freshly eluted ^{68}Ga in 0.1 M hydrogen chloride (pH=1) was mixed with an equal 1 M sodium acetate (pH=5). The radiometal solution with a final volume of 2 mL (pH=4.0–4.5) was added to 100–200 µg of NOTA-RW102 or NOTA-ABDRW102, followed by incubation of the mixture at 37°C for 5–10 min under constant shaking (600 rpm). For ^{89}Zr-labeling, the [^{89}Zr]Zr-oxalic acid solution (360 µL, 100 MBq) was mixed with 1 M Na_2CO_3 buffer solution (200 µL), resulting in a final pH=7 of the reaction. Then, pipette successively 300 µL of 0.5 M HEPES (pH=7.1–7.3) and 250 µL of DFO-ABDRW102 (500 µg) into the reaction vial and react at 37°C for 1 hour under constant shaking. For ^{64}Cu-labeling, $^{64}CuCl_2$ (111 MBq/3 mCi) was diluted in 300 µL of 0.1 M sodium acetate buffer (pH 5). The solution's pH was adjusted to a range of 4.5–5.5 and then added to 100–150 µg of ABDRW102, resulting in a total volume of less than 1 mL. The mixture was incubated for 1 hour at 37°C with constant shaking (600–800 rpm). The final radiopharmaceuticals were purified using equilibrated PD-10 columns, and the radiochemical purities were assessed by instant thin-layer chromatography (iTLC; Eckert & Ziegler Radiopharma).

Micro-PET/CT imaging, biodistribution, and histopathological studies

Small animal PET/CT imaging was performed using an integrated micro-PET/CT system (IRIS PET/CT, Inviscan, Strasbourg, France). Briefly, female nude mouse models were injected via the tail vein with radiolabeled probes and then anesthetized through inhalation of 2% isoflurane. Static imaging was obtained at 0.5–1 hours post-injection (p.i.). For blocking studies, unlabeled ABDRW102 (about 500 µg) was injected 2 days before the [^{68}Ga]Ga-NOTA-RW102 injection, leaving enough time to saturate PD-L1 molecules on tumor cells. The data were reconstructed using Monte-Carlo based three-dimensional ordered subset expectation maximization (Monte-Carlo based 3D OSEM). Images and regions of interest (ROIs) were processed using OsiriX Lite software (Pixmeo SARL) and Inveon Research Workplace (Siemens Preclinical Solutions). The mice were sacrificed after immunoPET imaging at the last time point. Samples, including blood, were collected and wet-weighed, and the radioactivity of the samples was counted using an automated γ-counter (PerkinElmer). The uptake value of %ID/g (mean±SD) was calculated and given for major organs and tissues. H&E and IHC staining of the fixed tissues were carried out to evaluate the expression level of human PD-L1. Briefly, sections of 10 µm were cut and stained for H&E and PD-L1 following the standard protocols. The antibody (Rabbit mAb #13684, Cell Signaling Technology) was used for IHC staining with a dilution

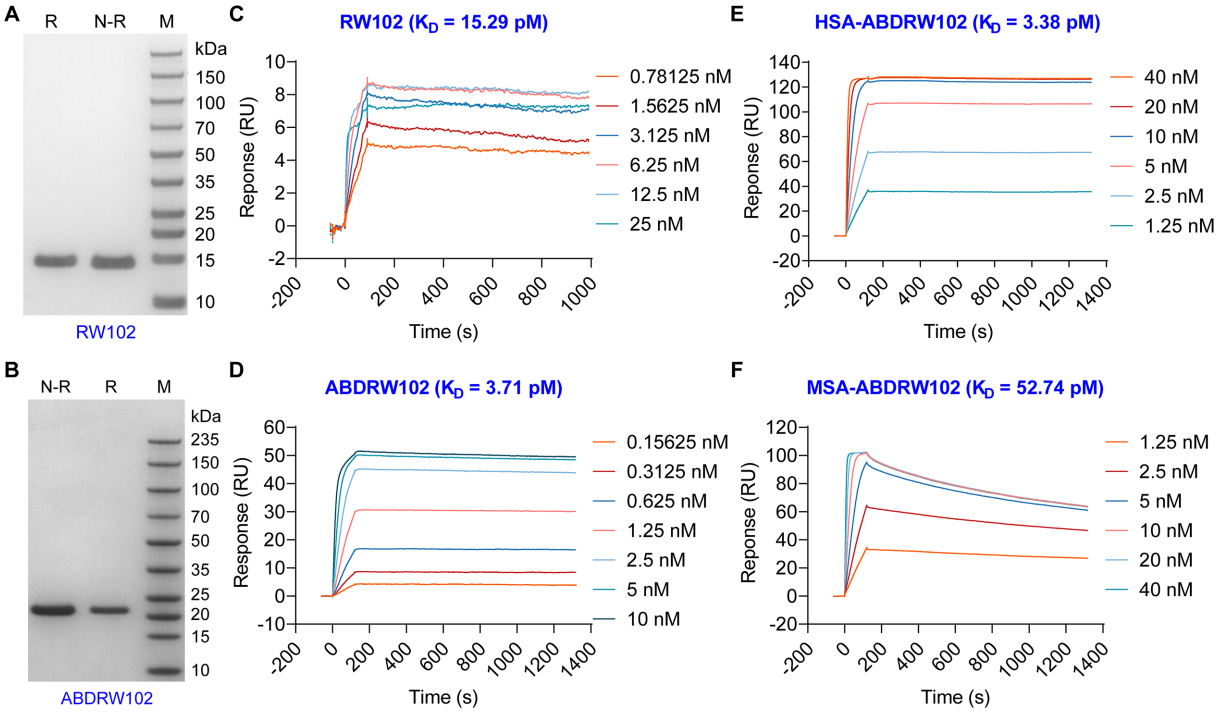

Figure 1 Characterization of RW102 and ABDRW102. The purity of RW102 (A) and ABDRW102 (B) examined by sulfate-polyacrylamide gel electrophoresis was >95%. (C and D) The surface plasmon resonance studies showed the association and dissociation kinetics of RW102 (C) and ABDRW102 (D) interacting with recombinant human programmed death receptor ligand 1 protein. (E and F) ABDRW102 also showed high binding affinities to human serum albumin (HSA, E) and murine serum albumin (MSA, F). M, marker; N-R, non-reducing condition; R, reducing condition.

rate 1:200. All the stained tissues were scanned for subsequent analysis.

Pilot translational study of [^{68}Ga]Ga-NOTA-RW102

RW102 was produced in CHO cells under good manufacturing practice conditions for clinical translational studies with endotoxin <1 EU/mg and purity >95%. The study was registered as a prospective clinical trial. The main objective of the clinical trial was to assess the safety and feasibility of [^{68}Ga]Ga-NOTA-RW102 immunoPET imaging. The participants enrolled were patients with NSCLC. Therefore, the secondary goal of the trial was to preliminarily explore the potential of [^{68}Ga]Ga-NOTA-RW102 immunoPET in visualizing PD-L1 expression in tumors, normal tissues, and organs, identifying patients suitable for PD-L1-targeted therapies and predicting irAEs. Written informed consents were obtained from all the included patients. [^{68}Ga]Ga-NOTA-RW102 safety was assessed through changes in laboratory test results, changes in vital signs, and summaries of adverse events (AE) before and after exposure to [^{68}Ga]Ga-NOTA-RW102. AE data were recorded according to National Cancer Institute Common Terminology Criteria for Adverse Events V.4.0.

Statistical analysis

Results are presented as mean value±SD. Statistical analyses were conducted using Prism V.8.3 statistical software (GraphPad Software). Multiple t-tests determined statistical significance for tumor volume between groups, and a p value of <0.05 was statistically significant.

RESULTS

Expression and characterization of RW102 and ABDRW102

Three PD-L1-targeting clones, RW101, RW102, and RW103, were expressed. The SDS-PAGE results showed that RW101 did not show a clear band (online supplemental figure S1A), RW103 had impure bands (online supplemental figure S1B), and RW102 had an excellent single band (>95%) (figure 1A). Fusing RW102 to the albumin binder ABD035 produces ABDRW102, exhibiting excellent purity on SDS-PAGE analysis (figure 1B). SPR analysis revealed that both the monovalent nanobody RW102 and the fused protein ABDRW102 could selectively bind to recombinant human PD-L1 with excellent KD values of 15.29 pM and 3.71 pM, respectively (figure 1C,D). The introduction of the ABD035 sequence in ABDRW102 resulted in a fourfold increase in binding affinity to human PD-L1. Besides, ABDRW102 has a high affinity with HSA and MSA, with corresponding KD value of 3.38 pM and 52.74 pM (figure 1E,F). As expected, random chelator conjugation of RW102 and ABDRW102 slightly impaired the binding affinities, but the measured K_D values were still within low picomoles. The calculated K_D value of NOTA-RW102, NOTA-ABDRW102, and DFO-ABDRW102 was 47.23 pM, 79.51 pM, and 105.6 pM, respectively (online supplemental figure S2). Moreover,

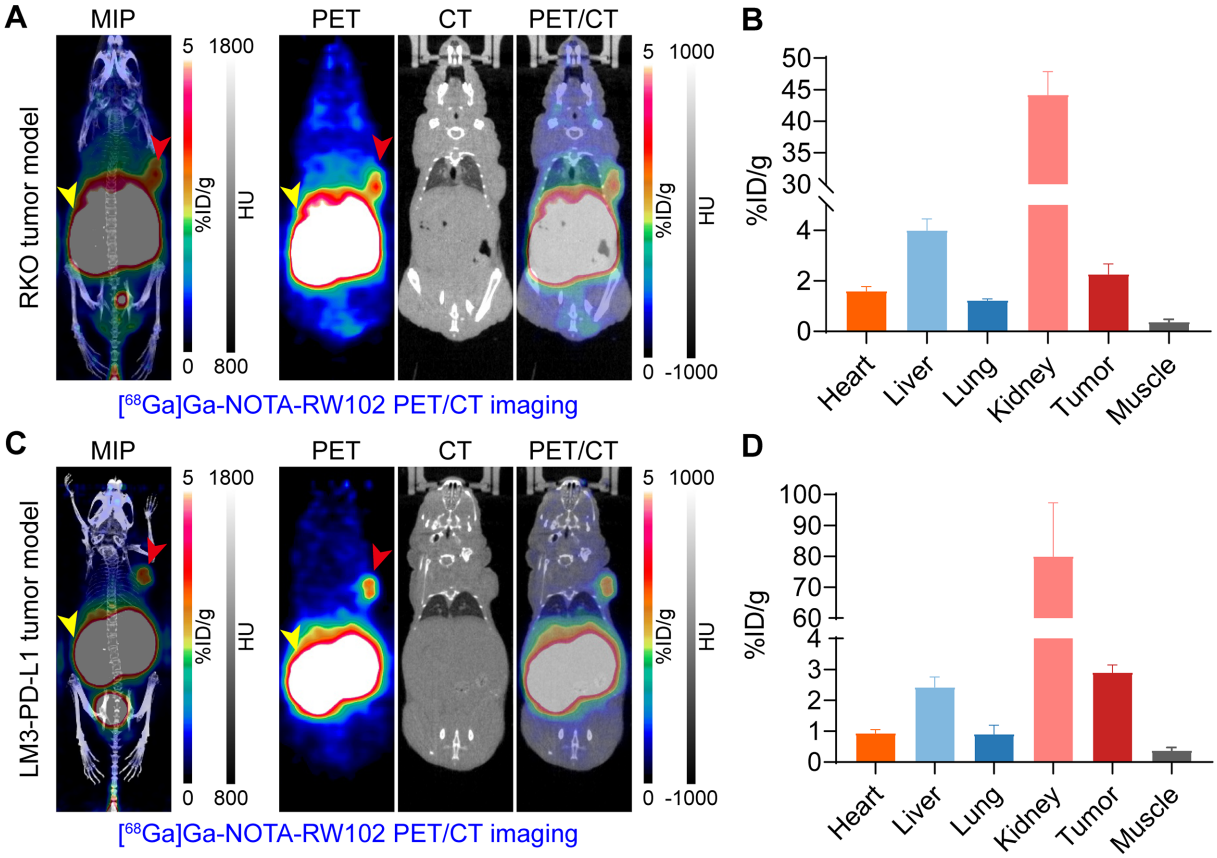

Figure 2 [^{68}Ga]Ga-NOTA-RW102 immunoPET imaging in subcutaneous tumor models. (A and C) [^{68}Ga]Ga-NOTA-RW102 immunoPET imaging in subcutaneous RKO (A, 7.64±1.42 MBq, n=3) and LM3-PD-L1 (C, 4.35±0.47 MBq, n=4) models 0.5 hours post-injection of the tracer. Maximum intensity projection (MIP) and coronal images showed clear delineation of the tumors (red arrowheads) and kidneys (yellow arrowheads), from which the tracer was excreted. (B and D) Quantitative data showed the tracer uptake and distribution patterns in RKO (B) and LM3-PD-L1 (D) models. immunoPET, immuno-positron emission tomography; PD-L1, programmed death receptor ligand 1.

RW102 had no apparent affinity with murine PD-L1 (online supplemental figure S3). These findings suggest that RW102 and ABDRW102 are ideal vectors for creating molecular imaging tracers that target PD-L1.

Preclinical [^{68}Ga]Ga-NOTA-RW102 immunoPET imaging in solid tumors

The non-decay corrected radiolabeling yield (RCY) and radiochemical purity (RCP) of [^{68}Ga]Ga-NOTA-RW102 assessed by iTLC was 70% and >99%, respectively (online supplemental figure S4). We screened the expression of PD-L1 in several tumors and found that the RKO model was PD-L1 positive (online supplemental figure S5). We first evaluated the diagnostic value of [^{68}Ga]Ga-NOTA-RW102 immunoPET in subcutaneous RKO (figure 2A,B) and LM3-PD-L1 (figure 2C,D) tumor models with high PD-L1 expression. As can be seen from the maximum intensity projection (MIP) and coronal images, [^{68}Ga]Ga-NOTA-RW102 was rapidly excreted from the kidneys after entering the circulation. Meanwhile, the tumors were readily delineated at half an hour after injection of the tracer, as indicated by the red arrowheads. As revealed by the ROI analysis (figure 2B,D), the average tumor uptake in the RKO and LM3-PD-L1 models was 2.27±0.33% ID/g (n=3) and 2.90±0.21% ID/g (n=4) while the target-to-muscle ratio was 6.11±0.66% ID/g (n=3) and 7.98±1.47% ID/g (n=4), respectively. In No. 62 PDX models (online supplemental figure S6A–C), where there is minimal expression of human PD-L1 on tumor cells and abundant expression of murine PD-L1 on neovascularisations, there was a slight uptake of [^{68}Ga]Ga-NOTA-RW102 at the tumor site. The calculated tumor uptake value was 0.80±0.06% ID/g (n=4). In T3-M4 with negative PD-L1 expression on tumor cells (online supplemental figure S6D–F), there was no apparent uptake of [^{68}Ga]Ga-NOTA-RW102 at the tumor site with the calculated tumor uptake value of 0.22±0.02% ID/g (n=4). The efficacy of [^{68}Ga]Ga-NOTA-RW102 immunoPET in detecting differential PD-L1 levels in solid tumors was demonstrated in the above data. However, further confirmation of its specificity is required.

Preclinical [^{68}Ga]Ga-NOTA-RW102 immunoPET imaging and blocking studies

The targeting specificity of [^{68}Ga]Ga-NOTA-RW102 was validated in the A375-PD-L1 tumor models. We performed two groups of experiments, that is, the control group and the ABDRW102 blocking group. The mice of the

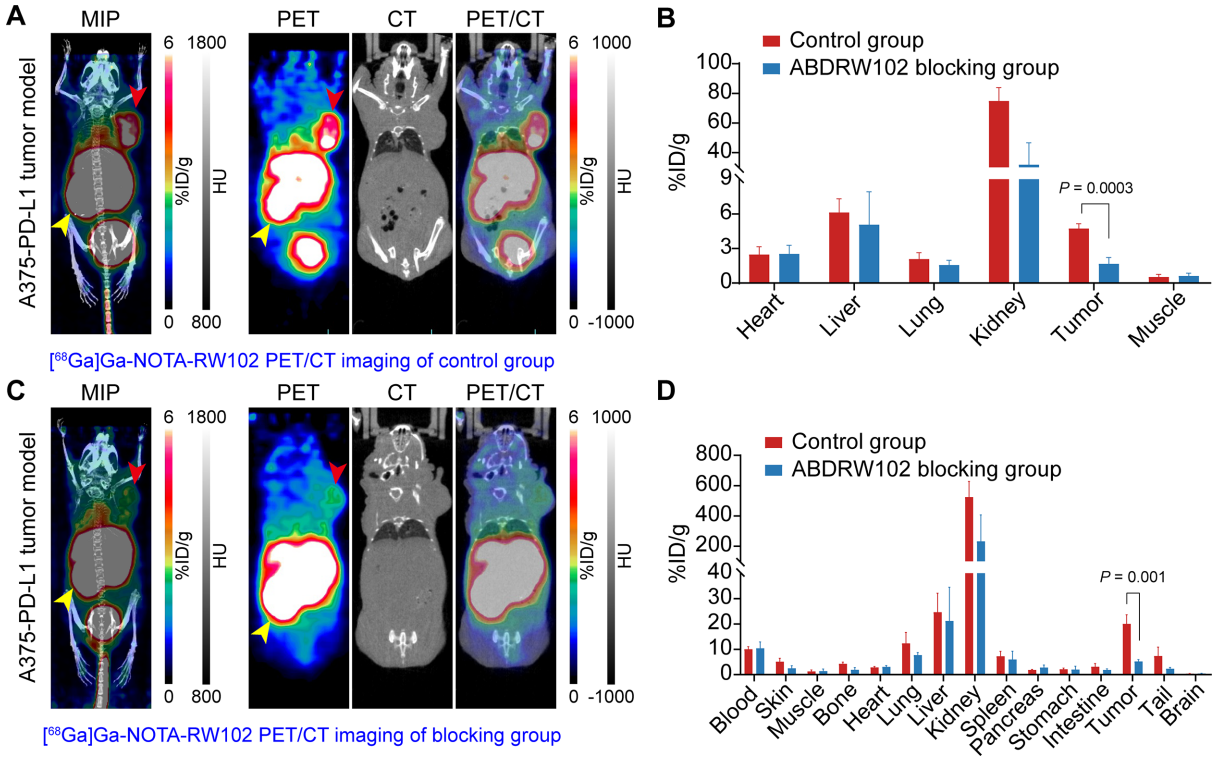

Figure 3 [^{68}Ga]Ga-NOTA-RW102 immunoPET imaging in A375-PD-L1 tumor models without or with ABDRW102 blocking. (A and C) [^{68}Ga]Ga-NOTA-RW102 immunoPET imaging in the control group (A) and ABDRW102 blocking group (C). (B) Quantitative regions of interest analysis results in the control group and ABDRW102 blocking group. (D) *Ex vivo* biodistribution data showed the detailed distribution and uptake patterns of [^{68}Ga]Ga-NOTA-RW102 in the control group and ABDRW102 blocking group. immunoPET, immuno-positron emission tomography; PD-L1, programmed death receptor ligand 1.

blocking group were injected with 500 µg of ABDRW102 2 days before injection of [^{68}Ga]Ga-NOTA-RW102, while the mice of the control group were injected with the same volume of saline. Similarly, the imaging was performed half an hour after injection of the tracer. As shown in figure 3A,C, the distribution and clearance patterns of the tracer were similar in both groups. However, the two groups had a significant difference in the tumor uptake. Specifically, the control group showed a significantly higher tumor uptake than the blocking group (p=0.0003). Based on the ROI data analysis (figure 3B), the tumor uptake value of the blocking group and the control group was 1.67±0.39% ID/g (n=3) and 4.73±0.32% ID/g (n=4), respectively. After immunoPET imaging, tumor-bearing mice were sacrificed for biodistribution experiments. The results showed that the tumor uptake value of the control group and the blocking group was 20.06±3.13% ID/g (n=4) and 5.23±0.57% ID/g (n=3), respectively (figure 3D). The difference was significant (p=0.001). The subsequent IHC data confirmed the positive expression of PD-L1 in the tumors (online supplemental figure S7), demonstrating the superior targeting specificity of [^{68}Ga]Ga-NOTA-RW102 for imaging PD-L1 expression levels.

[^{68}Ga]Ga-NOTA-ABDRW102 immunoPET imaging in colorectal cancer models

The TLC data indicated that [^{68}Ga]Ga-NOTA-ABDRW102 was synthesized with 91% RCY and >99% RCP (online supplemental figure S8). Adding ABD035 to nanbodies notably extends the *in vivo* circulation time.[18 20 21] Therefore, we conducted multiple immunoPET imaging of [^{68}Ga]Ga-NOTA-ABDRW102 at different time points (0.5–6 hours) in RKO tumor models (figure 4A). ROI analysis data revealed a gradual increase in tumor uptake over time (figure 4B), consistent with the increasing tumor uptake seen on PET images. The average tumor uptake at 0.5 hours, 2 hours, 4 hours, and 6 hours was 3.94±0.78% ID/g, 5.30±0.77% ID/g, 7.14±1.26% ID/g, and 8.38±1.26% ID/g (n=6), respectively. The t-test results showed a significant difference in tumor uptake value between 0.5 hours and 6 hours (p<0.0001). Notably, the probe retention in the blood pool (17.76±1.05% ID/g, n=6) of the tumor-bearing mice at 6 hours p.i. was still significantly higher than the tumor uptake (8.38±1.26% ID/g, n=6), suggesting the prolonged circulation time of the probe at least within 6 hours. In addition, kidney accumulation of [^{68}Ga]Ga-NOTA-ABDRW102 (11.5±0.54% ID/g, n=6) was significantly lower than that of [^{68}Ga]Ga-NOTA-RW102 (44.2±3.00% ID/g, n=3) at 0.5 hours p.i. The biodistribution data further confirmed the *in vivo* distribution patterns of the tracer (figure 4C). IHC staining of the collected tumor showed intense PD-L1 expression

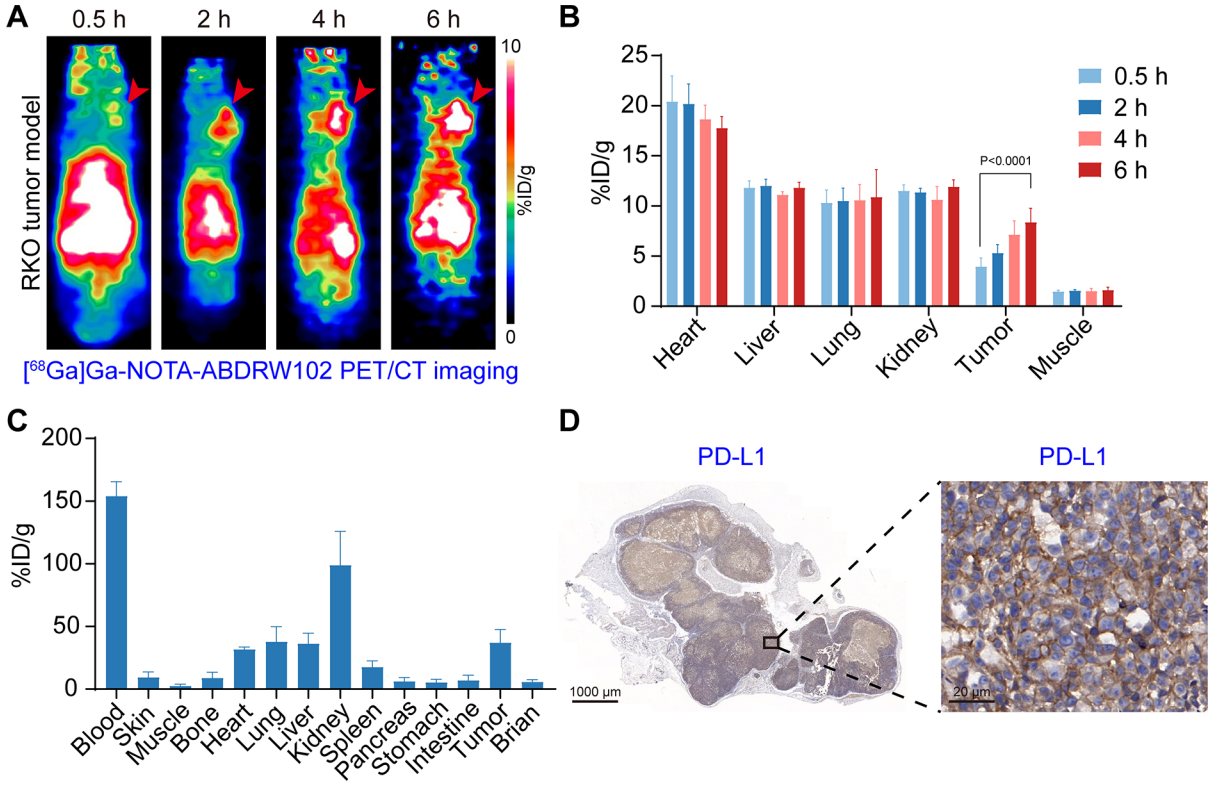

Figure 4 Serial [^{68}Ga]Ga-NOTA-ABDRW102 immunoPET imaging in RKO cancer models (5.87±0.27 MBq, n=6). (A) Representative PET images of [^{68}Ga]Ga-NOTA-ABDRW102 at multiple time points. The images showed clear delineation of the tumors (red arrowheads). (B) Regions of interest data of [^{68}Ga]Ga-NOTA-ABDRW102 immunoPET imaging at different time points. (C) *Ex vivo* biodistribution data showing the detailed uptake and distribution of [^{68}Ga]Ga-NOTA-ABDRW102 in the tumor, blood, major organs, and tissues. (D) Immunohistochemical verification of PD-L1 expression in tumors resected after immunoPET imaging. immunoPET, immuno-positron emission tomography; PD-L1, programmed death receptor ligand 1.

on the membranes of the tumor cells (figure 4D). To summarize, [^{68}Ga]Ga-NOTA-ABDRW102 has significantly extended circulation within the body and allows for non-invasive identification of PD-L1 expression in tumors. However, based on the quantitative analysis data of [^{68}Ga]Ga-NOTA-ABDRW102 (as shown in figure 4B,C), it is clear that the short half-life of ^{68}Ga ($T_{1/2}$=68.1 min) does not match that of ABDRW102. Therefore, radionuclides with a longer half-life are required to match the circulation time of ABDRW102.

[^{64}Cu]Cu-NOTA-ABDRW102 immunoPET imaging in colorectal cancer models

Of medical radionuclides with a long half-life, ^{124}I ($T_{1/2}$=68.1 min), ^{64}Cu ($T_{1/2}$=12.7 hours), and ^{89}Zr ($T_{1/2}$=78.4 hours) are favored because of their good availability. Therefore, we further developed [^{64}Cu]Cu-NOTA-ABDRW102 to investigate the diagnostic performance. This research sought to shed light on the dynamic behavior of this novel radiotracer at different time intervals following injection (figure 5A). Notably, analysis of TLC data underscored the successful radiolabeling process, yielding RCY >80%. Our PET/CT imaging analysis, through ROI assessments, unveiled a discernible trend in tracer accumulation within the tumor over time (figure 5B). Quantitatively, the average tumor uptake was recorded as 2.12±1.07% ID/g at 1 hour, 2.85±1.03% ID/g at 4 hours, 3.82±0.33% ID/g at 24 hours, and 3.22±0.27% ID/g at 48 hours p.i. (n=4). Statistically, a t-test revealed a remarkable difference in tumor uptake between the initial time point at 1 h and the later time point at 24 hours ($p<0.05$). IHC staining of tumor samples corroborated these findings, revealing a significant presence of PD-L1 expression on the tumor cell membranes. We further conducted biodistribution studies after the termination of the imaging, and the results demonstrated preferential accumulation of [^{64}Cu]Cu-NOTA-ABDRW102 in the tumors, followed by accumulation in the kidneys and circulation (figure 5C). Our study underscores the remarkable attributes of [^{64}Cu]Cu-NOTA-ABDRW102, characterized by an extended *in vivo* circulation period, thus enabling non-invasive and precise detection of PD-L1 expression within tumor models. Still, the retention of the tracer in circulation (3.99±0.27 %ID/g) based on biodistribution data indicates the need to use radionuclide of longer half-life to elucidate the circulation profiles of ABDRW102 thoroughly.

[^{89}Zr]Zr-DFO-ABDRW102 immunoPET imaging in PD-L1 positive cancer models

The data in the previous section show that there is still a high retention of [^{64}Cu]Cu-NOTA-ABDRW102 in the blood pool at 48 hours, suggesting a radionuclide with longer half-life is needed to trace the complete

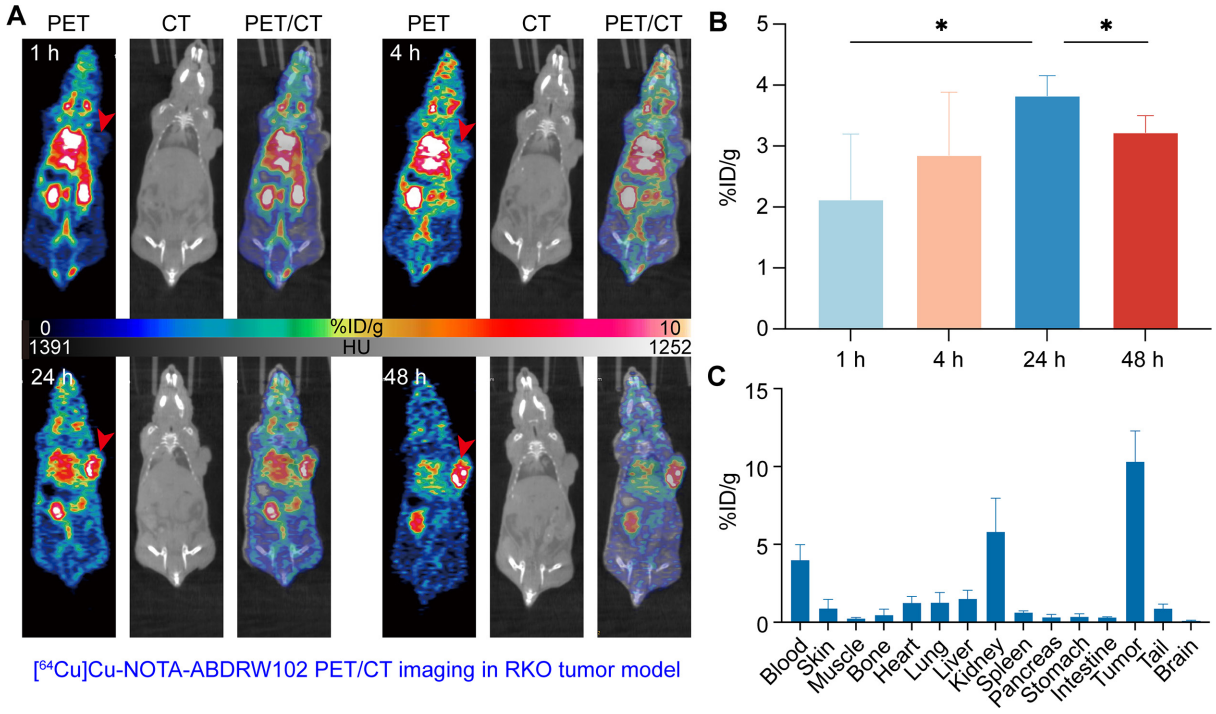

Figure 5 Serial [^{64}Cu]Cu-NOTA-ABDRW102 immunoPET imaging in RKO models. (A) Representative PET images of [^{64}Cu]Cu-NOTA-ABDRW102 at multiple time points. (B) Regions of interest data of [^{64}Cu]Cu-NOTA-ABDRW102 immunoPET imaging in tumors at different time points. (C) *Ex vivo* biodistribution data showed the detailed uptake and distribution of [^{64}Cu]Cu-NOTA-ABDRW102 in the tumor, blood, major organs, and tissues. immunoPET, immuno-positron emission tomography.

pharmacokinetics of ABDRW102 accurately. Hence, we used ^{89}Zr with a long half-life of 3.33 days and further developed [^{89}Zr]Zr-DFO-ABDRW102 with a good RCY of 85% and excellent RCP of 99% (online supplemental figure S9A,B). Imaging was performed at different intervals after injecting [^{89}Zr]Zr-DFO-ABDRW102 into LM3-PD-L1 tumor models. The MIP images (figure 6A, upper panel) showed that the uptake value at the tumor site gradually increased over time and reached its peak at 48 hours (5.20±0.70% ID/g, n=3). After that, the uptake value gradually decreased until 144 hours, when the cardiac shadow could no longer be seen on the MIP image. In addition, bone uptake did not increase until 144 hours, demonstrating the stability of the probe at each time point (online supplemental figure S9C,D). The curves plotted from the ROI data are consistent with gross findings in the MIP images (figure 6B, up panel). To demonstrate the targeting specificity of [^{89}Zr]Zr-DFO-ABDRW102, we conducted a blocking study in which mice were administered with 500 µg of ABDRW102 2 days before the injection of [^{89}Zr]Zr-DFO-ABDRW102. The results showed that the retention of [^{89}Zr]Zr-DFO-ABDRW102 in the blood pool of the mice gradually decreased over time, and there was no significant tracer uptake at the tumor site all the time (figure 6A, down panel), which is different from the control group. We also compared the tumor uptake in the two groups and showed significant differences in tumor uptake at each time point (figure 6C). Further biodistribution data confirmed the high tracer uptake at the tumor site in the control group (figure 6D). We also performed IHC staining of the resected tumors to confirm positive PD-L1 expression in the LM3-PD-L1 tumors (online supplemental figure S10).

[^{68}Ga]Ga-NOTA-RW102 immunoPET imaging in patients with NSCLCs

We translated [^{68}Ga]Ga-NOTA-RW102 for same-day PD-L1 imaging. Information on patients in the clinical trial was summarized in online supplemental table S1. No obvious AE and laboratory abnormalities were recorded in conducting the studies.

Our preliminary results show that [^{68}Ga]Ga-NOTA-RW102 immunoPET can non-invasively annotate PD-L1 expression in primary squamous lung cancer, as shown in figure 7A–C. Subsequently, the tumor's PD-L1 expression level was verified to be 70% by IHC staining (figure 7E). Another patient with multiple metastases from NSCLC underwent two imaging examinations of ^{18}F-FDG and [^{68}Ga]Ga-NOTA-RW102, respectively. While ^{18}F-FDG showed intense accumulation in all the lesions, [^{68}Ga]Ga-NOTA-RW102 showed negligible uptake (online supplemental figure S11). Further histopathological studies confirmed negative PD-L1 staining in primary tumor and mediastinal lymph node metastases (online supplemental figure S12). A patient with left lower lung adenocarcinoma, who was undergoing treatment with almonertinib mesilate (a tyrosine kinase inhibitor targeting EGFR^{T790M}), received [^{68}Ga]Ga-NOTA-RW102 immunoPET imaging. Although the primary tumor had shrunk and showed no significant tracer

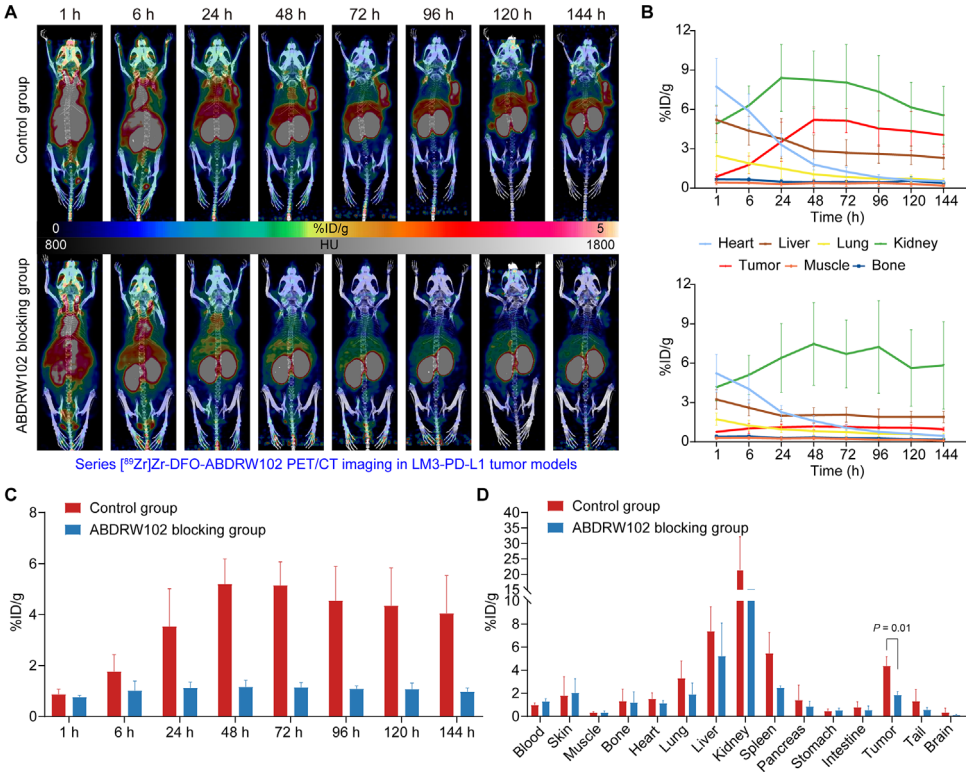

Figure 6 [^{89}Zr]Zr-DFO-ABDRW102 immuno-positron emission tomography imaging in LM3-PD-L1 models (2.66±0.74 MBq, n=8). (A) Maximum intensity projection PET/CT images of the control group (up panel) and ABDRW102 blocking group (down panel) at multi-time points. (B) Regions of interest data showed the uptake kinetics of [^{89}Zr]Zr-DFO-ABDRW102 in the control group and ABDRW102 blocking group at different time points. (C) Comparison of tumor uptake value between the control and ABDRW102 blocking groups at each time point. (D) *Ex vivo* biodistribution data showed the detailed uptake and distribution of [^{89}Zr]Zr-DFO-ABDRW102 in the control and ABDRW102 blocking groups. PD-L1, programmed death receptor ligand 1; PET, positron emission tomography.

uptake, the imaging revealed diffuse tracer accumulation in the bilateral thyroid lobes (online supplemental figure S13). The patient had increased levels of thyroid-stimulating hormone (TSH, 6.04 mIU/L), thyroglobulin antibody (TgAb, 271.0 U/mL), and thyroid peroxidase antibody (TPOAb, 99.4 U/mL), confirming the presence of thyroiditis. We observed no significant difference in SUVmax between patients with PD-L1 expression less

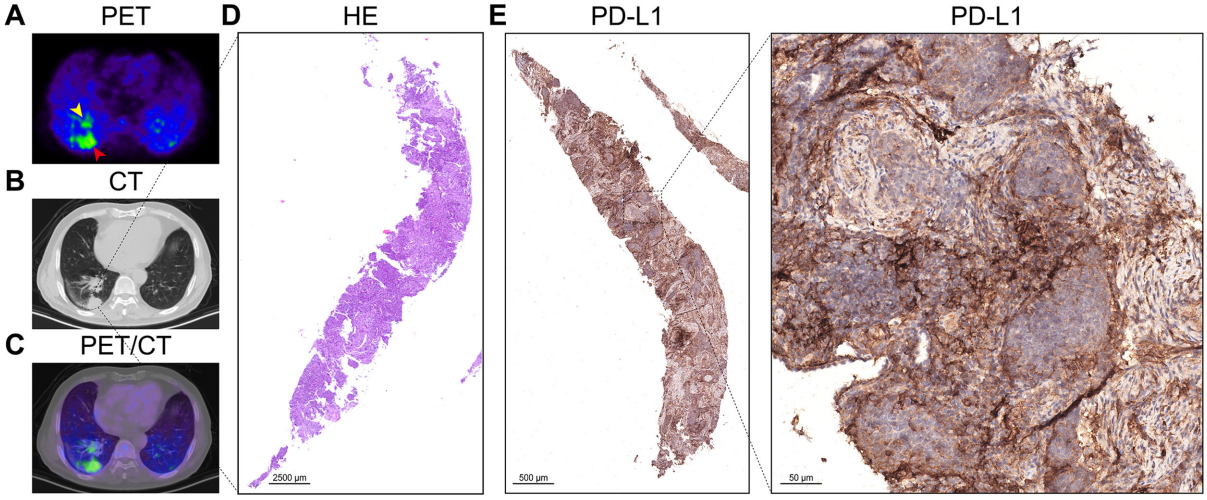

Figure 7 [^{68}Ga]Ga-NOTA-RW102 immuno-positron emission tomography imaging of an adult patient with squamous lung cancer with 70% PD-L1 expression. (A–C) [^{68}Ga]Ga-NOTA-RW102 PET/CT images of two tumor lesions in this patient (yellow and red arrowheads). (D) The H&E staining of the subpleural lesion in the lower lobe of the patient's right lung. (E) The PD-L1 staining of the biopsied squamous lung cancer tissue showed 70% positivity. PD-L1, programmed death receptor ligand 1; PET, positron emission tomography.

than or equal to 10% and those with greater than 10% (online supplemental figure S14A). This result is likely due to the small sample size, requiring further validation in larger cohorts. The characteristics of [^{68}Ga]Ga-NOTA-RW102 uptake in different organs are presented in online supplemental figure S14B. The preliminary data suggest that [^{68}Ga]Ga-NOTA-RW102 immunoPET can visualize differential PD-L1 in NSCLCs. ImmunoPET using [^{68}Ga]Ga-NOTA-RW102 may help monitor inflammatory conditions like thyroiditis, but further studies are needed to confirm the application value.

DISCUSSION

PD1/PD-L1-targeted immunotherapies have greatly improved cancer management. Despite the progress, there is still room for improving the clinical administration of antibody therapeutics by precisely monitoring PD-L1 dynamics in the tumor and across the body. With the stride in molecular imaging, several tracers have entered early-phase clinical trials to non-invasively visualize PD-L1 expression, including mAb tracers (eg, ^{89}Zr-atezolizumab and ^{89}Zr-durvalumab),[7 22] adnectin tracers,[23 24] peptide tracers,[25–28] and also nanobody tracers.[9 10] PD-L1 expression is abundant in subsets of immune cells in healthy lymphoid tissues, resulting in high accumulation of PD-L1-targeted tracers in the spleen.[7 29] However, preclinical and clinical data showed that WL12-derived tracers had low spleen uptake and high liver accumulation[26]; similar results went to ^{18}F-NOTA-NF12.[27] Whether or not the varying pharmacokinetic profile potentially affects their diagnostic efficacies needs to be elucidated. In general, sufficient antibody concentrations are required to overcome distribution to PD-L1-positive normal tissues to provide circulating tracer levels needed for specific tumor accumulation.[30]

Cowles *et al* elucidated that higher affinity correlated with increased target saturation in the case of anti-PD-1 antibodies.[31] The K_D value of the reported PD-L1 tracers ranges from 328.0 to 2.0 nM. We assumed that high or ultra-high affinity tracers can rapidly detect PD-L1 expressed at low abundance. Therefore, we successfully screened a PD-L1 nanobody (ie, RW102) with an ultra-high K_D value of 15.29 pM, assuring efficient detection of low-level PD-L1 expression. Albumin hitchhiking is a valuable strategy to prolong circulation and enhance the tumor uptake of small-molecule inhibitors and biologics.[32] We previously showed that incorporating albumin binder ABD035 into Glypican 3-targeting nanobody significantly increased tumor uptake and decreased kidney accumulation of the developed radiotracer.[33] We have engineered ABDRW102 to bind simultaneously to human and murine albumins and human PD-L1. The binding is ultra-strong with corresponding K_D value of 3.38 pM, 52.74 pM, and 3.71 pM, respectively. This allows the development of long-lived [^{64}Cu]Cu-NOTA-ABDRW102 and [^{89}Zr]Zr-DFO-ABDRW102 due to prolonged circulation. In RKO models, the tumor uptake of [^{64}Cu]Cu-NOTA-ABDRW102 was higher than that of the parent tracer [^{68}Ga]Ga-NOTA-RW102. [^{89}Zr]Zr-DFO-ABDRW102 had excellent *in vivo* stability, as indicated by low bone uptake and specificity, and reduced tumor uptake after cold ABDRW102 blocking.

We and others are actively advocating the incorporation of molecular imaging toolbox in molecularly targeted therapies and cancer immunotherapies.[1 34 35] The current translational study has shown the roadmap for developing and translating PD-L1-targeted tracers, especially the [^{68}Ga]Ga-NOTA-RW102. Although the SUVmax of the patient with 70% PD-L1 expression was only 5.45, the preliminary pilot study has shown the promising value of [^{68}Ga]Ga-NOTA-RW102 in delineating varying PD-L1 expression in NSCLC. Low tumor uptake of [^{68}Ga]Ga-NOTA-RW102 may be due to short circulating time and natural PD-L1 expression in normal organs and tissues. Additionally, we are still uncertain about how the injection dosage will affect the tracer's distribution profiles. Furthermore, we are currently enrolling patients to examine the effectiveness of [^{68}Ga]Ga-NOTA-RW102 in demonstrating PD-L1 expression and identifying patients who may benefit from PD-L1-targeted therapies. The irAEs include pneumonitis, colitis, hepatitis, pancreatitis, thyroiditis, hypophysitis, synovitis, arthritis, and even sarcoid-like granulomatosis and lymphadenopathy.[36 37] However, there are limited tools to characterize and monitor systemic irAEs. Our initial data showed that [^{68}Ga]Ga-NOTA-RW102 has the potential to predict or monitor thyroiditis. Future efforts are needed to explore the value of the tracer in predicting or monitoring irAEs.

^{68}Ga-NOTA-WL12 is a peptide tracer targeting human PD-L1 that has already been translated for clinical use.[26] Therefore, we are also conducting a clinical trial comparing the differential diagnostic values of [^{68}Ga]Ga-NOTA-RW102 and ^{68}Ga-NOTA-WL12 in patients with NSCLC. Moreover, PD-L1 is a multifaceted molecule aside from its role in mediating the immune system. For instance, PD-L1 is an activation-independent marker of brown fat, and PD-L1-targeted PET imaging efficiently identified small brown adipose deposits.[38] As a part of the PD-L1-targeted molecular imaging toolbox, [^{68}Ga]Ga-NOTA-RW102 may find its value in diverse research fields and clinical application scenarios.

Author affiliations
[1]Department of Nuclear Medicine, Institute of Clinical Nuclear Medicine, Renji Hospital, School of Medicine, Shanghai Jiao Tong University, Shanghai, China
[2]Department of Thoracic Surgery , Renji Hospital, School of Medicine, Shanghai Jiao Tong University, Shanghai, China
[3]Department of Nuclear Medicine & PET Center, Huashan Hospital, Fudan University, Shanghai, China
[4]Departments of Radiology and Medical Physics, University of Wisconsin–Madison, Madison, Wisconsin, USA
[5]Department of Medical Biotechnology, Faculty of Medical Sciences, Tarbiat Modares University, Tehran, Iran
[6]Department of Thoracic Surgery, Huashan Hospital Fudan University, Shanghai, China
[7]Department of Nuclear Medicine, Fudan University Shanghai Cancer Center, Shanghai, China

Acknowledgements We thank colleagues at our hospitals for helpful discussions in carrying out the studies.

Contributors WW, FX, and W. Cai collaboratively conceived and designed the project. YZ, YW, EY, SM, and MHY performed the experiments. MC and QL analyzed and interpreted the clinical data. YZ, MC, and WW wrote most of the manuscript while others contributed to the writing. CW and HZ produced 89Zr used in preclinical studies. WL and JWE produced 64Cu used in preclinical studies. YG, GH, MJR, and JL provided inputs in the initial design of the project and revised the manuscript. WW, FX, and W. Cai supervised the study, revised, and finalized the manuscript. WW acts as the guarantor of this work.

Funding This work was supported in part by the National Key Research and Development Program of China (Grant No. 2020YFA0909000), the National Natural Science Foundation of China (Grant No. 82372014 and 82171972), the University of Wisconsin – Madison, and the National Institutes of Health (P30 CA014520 and T32 CA009206).

Competing interests WW, YZ and JL are inventors of a pending patent describing the reported PD-L1 tracers. WW is a consultant of Alpha Nuclide (Ningbo) Medical Technology Co., Ltd. WC declares conflict of interest with the following corporations: Actithera, Inc., Portrai, Inc., rTR Technovation Corporation, Four Health Global Pharmaceuticals Inc., and POP Biotechnologies, Inc.

Patient consent for publication Consent obtained directly from patient(s).

Ethics approval This study involves human participants and was approved by Institutional Ethic Reviewing Board of Huashan Hospital (2023-546). Participants gave informed consent to participate in the study before taking part.

Provenance and peer review Not commissioned; externally peer reviewed.

Data availability statement Data are available upon reasonable request. Additional data are available from WW upon reasonable request.

ORCID iDs
Haitao Zhao http://orcid.org/0000-0002-8765-3690
Weijun Wei http://orcid.org/0000-0003-3190-2480

REFERENCES

1 Wei W, Rosenkrans ZT, Liu J, *et al*. Immunopet: concept, design, and applications. *Chem Rev* 2020;120:3787–851.
2 Chakravarty R, Goel S, Cai W. Nanobody: the "magic bullet" for molecular imaging. *Theranostics* 2014;4:386–98.
3 Rashidian M, Ploegh H. Ploegh H: Nanobodies as noninvasive imaging tools. *Immunooncol Technol* 2020;7:2–14.
4 Wei W, Younis MH, Lan X, *et al*. Single-domain antibody theranostics on the horizon. *J Nucl Med* 2022;63:1475–9.
5 Keyaerts M, Xavier C, Heemskerk J, *et al*. Phase I study of 68Ga-HER2-Nanobody for PET/CT assessment of HER2 expression in breast carcinoma. *J Nucl Med* 2016;57:27–33.
6 D'Huyvetter M, Vos JD, Caveliers V, *et al*. Phase I trial of (131) I-GMIB-anti-HER2-VHH1, a new promising candidate for HER2-targeted radionuclide therapy in breast cancer patients. *J Nucl Med* 2021;62:1097–105.
7 Bensch F, van der Veen EL, Lub-de Hooge MN, *et al*. (89)Zr-Atezolizumab imaging as a noninvasive approach to assess clinical response to PD-L1 blockade in cancer. *Nat Med* 2018;24:1852–8.
8 Hirsch FR, McElhinny A, Stanforth D, *et al*. PD-L1 immunohistochemistry assays for lung cancer: results from phase 1 of the blueprint PD-L1 IHC assay comparison project. *J Thorac Oncol* 2017;12:208–22.
9 Xing Y, Chand G, Liu C, *et al*. Early phase I study of a (99M)Tc-labeled anti-programmed death Ligand-1 (PD-L1) single-domain antibody in SPECT/CT assessment of PD-L1 expression in non-small cell lung cancer. *J Nucl Med* 2019;60:1213–20.
10 Lv G, Sun X, Qiu L, *et al*. PET imaging of tumor PD-L1 expression with a highly specific nonblocking single-domain antibody. *J Nucl Med* 2020;61:117–22.
11 Yang Y, Wang C, Wang Y, *et al*. Dose escalation biodistribution, positron emission tomography/computed tomography imaging and dosimetry of a highly specific radionuclide-labeled non-blocking Nanobody. *EJNMMI Res* 2021;11:113.
12 Bridoux J, Broos K, Lecocq Q, *et al*. Anti-human PD-L1 Nanobody for Immuno-PET imaging: validation of a conjugation strategy for clinical translation. *Biomolecules* 2020;10:1388.
13 Li D, Cheng S, Zou S, *et al*. Immuno-PET imaging of 89Zr labeled anti-PD-L1 domain antibody. *Mol Pharm* 2018;15:1674–81.
14 He H, Qi X, Fu H, *et al*. Imaging diagnosis and efficacy monitoring by [^{89}Zr]Zr-DFO-Kn035 immunoPET in patients with PD-L1-positive solid malignancies. *Theranostics* 2024;14:392–405.
15 Tison A, Garaud S, Chiche L, *et al*. Immune-checkpoint inhibitor use in patients with cancer and pre-existing autoimmune diseases. *Nat Rev Rheumatol* 2022;18:641–56.
16 Thompson JA, Schneider BJ, Brahmer J, *et al*. Management of immunotherapy-related toxicities, version 1.2022, NCCN clinical practice guidelines in oncology. *J Natl Compr Canc Netw* 2022;20:387–405.
17 Fecher LA, Bishu S, Fontana RJ, *et al*. The role of tissue biopsy in the management of immune checkpoint inhibitor toxicity. *J Natl Compr Canc Netw* 2022;20:417–25.
18 Zhang Y, Zhang D, An S, *et al*. Development and characterization of Nanobody-derived Cd47 Theranostic pairs in solid tumors. *Research* 2023;6:0077.
19 Avila-Rodriguez MA, Nye JA, Nickles RJ. Simultaneous production of high specific activity 64Cu and 61Co with 11.4 Mev protons on enriched 64Ni nuclei. *Appl Radiat Isot* 2007;65:1115–20.
20 Garousi J, von Witting E, Borin J, *et al*. Radionuclide therapy using ABD-fused ADAPT scaffold protein: proof of principle. *Biomaterials* 2021;266:120381.
21 Tijink BM, Laeremans T, Budde M, *et al*. Improved tumor targeting of anti-epidermal growth factor receptor Nanobodies through albumin binding: taking advantage of modular Nanobody technology. *Mol Cancer Ther* 2008;7:2288–97.
22 Smit J, Borm FJ, Niemeijer A-LN, *et al*. PD-L1 PET/CT imaging with Radiolabeled Durvalumab in patients with advanced-stage non-small cell lung cancer. *J Nucl Med* 2022;63:686–93.
23 Niemeijer AN, Leung D, Huisman MC, *et al*. Whole body PD-1 and PD-L1 positron emission tomography in patients with non-small-cell lung cancer. *Nat Commun* 2018;9:4664.
24 Robu S, Richter A, Gosmann D, *et al*. Synthesis and Preclinical evaluation of a 68Ga-labeled Adnectin, 68Ga-BMS-986192, as a PET agent for imaging PD-L1 expression. *J Nucl Med* 2021;62:1228–34.
25 Kumar D, Lisok A, Dahmane E, *et al*. Peptide-based PET quantifies target engagement of PD-L1 Therapeutics. *J Clin Invest* 2019;129:122216:616–30.:.
26 Zhou X, Jiang J, Yang X, *et al*. First-in-humans evaluation of a PD-L1-binding peptide PET radiotracer in non-small cell lung cancer patients. *J Nucl Med* 2022;63:536–42.
27 Zhou M, Wang X, Chen B, *et al*. Preclinical and first-in-human evaluation of (18)F-labeled D-peptide antagonist for PD-L1 status imaging with PET. *Eur J Nucl Med Mol Imaging* 2022;49:4312–24.
28 Hu K, Wu W, Xie L, *et al*. Whole-body PET tracking of a d-Dodecapeptide and its Radiotheranostic potential for PD-L1 overexpressing tumors. *Acta Pharmaceutica Sinica B* 2022;12:1363–76.
29 Kist de Ruijter L, Hooiveld-Noeken JS, Giesen D, *et al*. First-in-human study of the Biodistribution and pharmacokinetics of 89Zr-CX-072, a novel Immunopet Tracer based on an anti-PD-L1 Probody. *Clin Cancer Res* 2021;27:5325–33.
30 Bouleau A, Nozach H, Dubois S, *et al*. Optimizing Immuno-PET imaging of tumor PD-L1 expression: pharmacokinetic, Biodistribution, and Dosimetric comparisons of (89)Zr-labeled anti-PD-L1 antibody formats. *J Nucl Med* 2022;63:1259–65.
31 Cowles SC, Sheen A, Santollani L, *et al*. An affinity threshold for maximum efficacy in anti-PD-1 immunotherapy. *MAbs* 2022;14:2088454.
32 Jonsson A, Dogan J, Herne N, *et al*. Engineering of a femtomolar affinity binding protein to human serum albumin. *Protein Eng Des Sel* 2008;21:515–27.

33 An S, Zhang D, Zhang Y, *et al*. Gpc3-targeted immunoPET imaging of hepatocellular carcinomas. *Eur J Nucl Med Mol Imaging* 2022;49:2682–92.
34 van de Donk PP, Oosting SF, Knapen DG, *et al*. Molecular imaging to support cancer immunotherapy. *J Immunother Cancer* 2022;10:e004949.
35 Wu Q, Yang S, Liu J, *et al*. Antibody theranostics in precision medicine. *Med* 2023;4:69–74.
36 Kuchroo JR, Hafler DA, Sharpe AH, *et al*. The double-edged sword: harnessing PD-1 blockade in tumor and autoimmunity. *Sci Immunol* 2021;6:65.
37 Chiloiro S, Bianchi A, Giampietro A, *et al*. The changing clinical spectrum of endocrine adverse events in cancer immunotherapy. *Trends Endocrinol Metab* 2022;33:87–104.
38 Ingram JR, Dougan M, Rashidian M, *et al*. PD-L1 is an activation-independent marker of brown adipocytes. *Nat Commun* 2017;8.